Journal of Power Sources 245 (2014) 154–163

Contents lists available at SciVerse ScienceDirect

Journal of Power Sources

journal homepage: www.elsevier.com/locate/jpowsour

Optimization of dry reforming of methane over Ni/YSZ anodes for solid oxide fuel cells

Cosimo Guerra [a,*], Andrea Lanzini [a], Pierluigi Leone [a], Massimo Santarelli [a], Nigel P. Brandon [b]

[a] Department of Energy, Politecnico di Torino, Corso Duca degli Abbruzzi 24, 10129, Torino, Italy
[b] Department of Earth Science and Engineering, Imperial College, South Kensington Campus, London SW7 2AZ, United Kingdom

HIGHLIGHTS

- The catalytic activity of Ni/YSZ anodes under dry reforming of methane is studied.
- At 800 °C, the best performances are for 1.5 < carbon dioxide/methane (vol. ratio) < 2.
- Dry reforming and reverse water gas shift are the dominant reactions.
- Conversion is poor for both T < 450 °C and carbon dioxide/methane <1 at 800 °C.
- Stable conversion performance is maintained over a test period of 70 h.

GRAPHICAL ABSTRACT

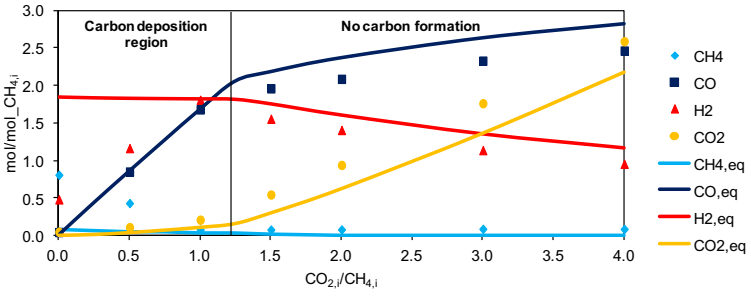

ARTICLE INFO

Article history:
Received 4 March 2013
Received in revised form
15 May 2013
Accepted 14 June 2013
Available online 26 June 2013

Keywords:
Reforming
Ni/YSZ SOFC anode
Methane
Carbon dioxide
Biogas
Catalytic properties

ABSTRACT

This work investigates the catalytic properties of Ni/YSZ anodes as electrodes of Solid Oxide Fuel Cells (SOFCs) to be operated under direct dry reforming of methane. The experimental test rig consists of a micro-reactor, where anode samples are characterized. The gas composition at the reactor outlet is monitored using a mass spectrometer. The kinetics of the reactions occurring over the anode is investigated by means of Isotherm reactions and Temperature-programmed reactions. The effect of the variation of temperature, gas residence time and inlet carbon dioxide–methane volumetric ratio is analyzed. At 800 °C, the best catalytic performance (in the carbon safe region) is obtained for 1.5 < carbon dioxide/methane ratio < 2, which is an interesting result for prospective direct biogas fueled SOFCs. Conversion is stable over a period of 70 h. Both for temperatures lower than 450 °C and for carbon dioxide–methane ratios lower than equi-molar at 800 °C, conversion is poor due to low activity of the anode toward dry reforming and cracking reactions, respectively. In other ranges, dry reforming and reverse water gas shift are the dominant reactions and the inlet feed reaches almost the equilibrium condition provided that a sufficient gas residence time is obtained.

1. Introduction

Solid oxide fuel cells (SOFCs) are attractive energy conversion systems due to the high electrical efficiency, the scalability in electricity generation applications and the low level of pollution produced during operation. Hence, SOFC based power systems are ideal as distributed power generation systems [1]. The ability of SOFCs to utilize CO as a fuel, rather than being poisoned, and their general fuel flexibility are some of the advantages of these systems, compared to lower temperature fuel cells [2–4]. Although some studies show the possibility of operating SOFCs at temperatures lower than 600 °C [5–7] (which could lower the cost of balance of

* Corresponding author. Tel.: +39 0110904422; fax: +39 0110904499.
E-mail addresses: cosimoguerra1@gmail.com, c.guerra11@imperial.ac.uk, cosimo.guerra@polito.it (C. Guerra).

0378-7753/$ – see front matter © 2013 Elsevier B.V. All rights reserved.
http://dx.doi.org/10.1016/j.jpowsour.2013.06.088

plant components), the operating temperature is usually set to 600–800 °C to reach sufficiently high ionic conductivity in the electrolyte material [8–12]. Nevertheless, the higher operating temperatures are an advantage to promote direct internal reforming reactions of hydrocarbon-based fuels and alcohols on the anode surface of the SOFC, to generate hydrogen and carbon monoxide for electrochemical oxidation at the anode [13]. The direct heat exchange between the exothermic electrochemical reactions and the endothermic reforming reactions is one of the main advantages of the direct internal reforming configuration, along with its potential to increase the overall system efficiency and to minimize reforming components [14]. Many available anode materials for SOFCs investigated in the last decades show interesting features and show promising results. Some examples are CeO_2 [15], Cu-based (e.g., Cu/YSZ or Cu/CeO_2/YSZ) [16–19], Ceria-supported precious metals (Pd/Ceria), perovskites [20,21], and thin layers of active SOFC components (e.g., Cu/YSZ) onto a porous metal support structure (e.g. stainless steel) [22]. However, the most used materials for the-state-of-art SOFCs remain Ni/YSZ ceramic-metallic (cermet) porous composites: Ni–YSZ has low cost, well matched thermal expansion requirements with the YSZ electrolyte, is relatively simple to fabricate and shows good electrochemical reactivity, electronic conductivity and catalytic activity toward reforming of hydrocarbon-based fuels at temperature higher than 700 °C. However, direct internal reforming of hydrocarbon fuels over Ni/YSZ often results in carbon deposition at the anode surface. Deposited solid carbon leads to degradation in anode performance due to deactivation of the nickel catalyst, inhibition of fuel diffusion and, in some cases, it can also dissolve into and block active sites on the nickel surface. Partial delamination of the anode surface from the electrolyte, and nickel particle agglomeration, can also occur in long-term operation, impacting on performances and stability [23–26]. The carbon deposition mechanism on Ni-based catalysts has been extensively investigated, showing that residence time, operating temperature, catalyst microstructure, and the addition of oxidant to the reactive feed, all have a strong impact on the catalytic activities [26–31].

Many efforts are devoted to improving Ni-based anodes in order to reach high stability and activity in the direct internal reforming of hydrocarbon-based fuels, while avoiding coking [32]: strategies tested include the addition of CaO to the Ni/YSZ cermet [31], the deposition of a film of yttria doped ceria (YDC) on the Ni/YSZ anode [33], the replacement of YSZ with scandia-stabilized zirconia (ScSZ) [34,35], the partial or total replacement of doped zirconia with CeO_2 [2,36], Ce/ZrO_2 [37], CGO [38], the replacement of doped zirconia by perovskites [39], and the partial replacement of Ni by precious metals (Pt, Pd, Ru) [40].

Some studies show that a sufficiently high cell current can prevent carbon deposition for a cell directly fed by dry methane [41] or by methane with 3% H_2O with Ni/YSZ anodes [42,43], or even by higher hydrocarbons using composite anodes of copper and ceria (or Samaria-doped ceria) [44]. This behavior is probably due to a combination of the backflow of the electrochemical reaction products (steam and carbon dioxide), which increases the local concentration of oxidant and reduces the methane partial pressure to values where coking is avoided [42,43,45], and direct oxidation of carbon deposited on the anode. Nevertheless, the presence of local temperature gradients, and the non-homogeneous distribution of the reactants and products of the electrochemical reactions, can produce local concentrations of solid carbon, even when carbon formation is not thermodynamically predicted [2,30]. Therefore, a significant amount of reforming agent (air, steam or carbon dioxide) is often used in long term operation to avoid carbon formation, especially in the presence of hydrocarbons higher than methane given that the catalytic activity of Ni for carbon formation is usually higher for these molecules. Steam is the most commonly used oxygen carrier to avoid deleterious reactions leading to carbon build-up on the anode surface. However, the need to provide the cell with steam, if not coming from other processes, or from the (partial) recirculation of the anode exhaust, decreases the global efficiency of the system [23,46], and can add complexity to the system design and control. Laosiripojana et al. show in their experiments that methane and methanol, with an appropriate steam content (H_2O/fuel = 3 vol. ratio), can be directly fed to a Ni/YSZ anode at 975 °C and 1000 °C respectively, without the problem of carbon formation. Otherwise, ethanol cannot be used as the direct fuel even at high steam contents and high operating temperatures [47]. Kinetic models for steam reforming reactions over Ni catalyst are proposed in recent studies [48,49] and the detailed analysis of the carbon formation boundaries for steam reforming of methane is reported in others [30,50]. Carbon dioxide reforming, also known as dry reforming, is another interesting and less exploited option than steam reforming for SOFCs, with thermodynamic characteristics similar to steam reforming, except that there is a greater potential for carbon formation, primarily due to the lower H/C ratio of the feeding mixture [51] and the significant surface coverage of carbon monoxide over the catalyst surface [49]. Experimental results on the durability for Ni/YSZ and Ni/ScSZ anodes examined in comparison with internal steam and dry reforming of methane confirm a higher order of degradation for the latter process [34]. Although the mechanism of dry reforming is still not fully understood, and different reaction paths are reported in literature [51–54], it is clear that the development of an effective catalyst is crucial to ensure that the methane dissociation and the carbon dioxide activation steps are not out of balance to optimize the catalytic conversion mechanism, and avoid carbon deposition phenomena.

Yentekakis et al. [55] show that the highest cell performances are for the equi-molar carbon dioxide–methane ratio over Ni(Au)/GDC and Ni/YSZ anodes at 875 °C; this result is consistent with other work [56], which has reported the maximum methane consumption rate for the same molar ratio with a NiO–ScSZ anode at 900 °C. In another paper [57], the maximum performance of a Ni/YSZ anode supported tubular SOFC working at 850 °C has been obtained for 45% of methane in a carbon dioxide–methane mixture (again, almost an equi-molar ratio). Experiments performed over a Ni/YSZ cermet anode supported SOFC with an equi-molar mixture at 800 °C have shown power density values very close to those of humidified hydrogen [58]. However, an equi-molar ratio of carbon dioxide and methane produces solid carbon on the anode surface in open circuit condition at 1 atm and temperature at or above 800 °C. A reduction in temperature dramatically increases the required inlet carbon dioxide–methane ratio. Detailed thermodynamic analyses on the boundary of carbon formation in SOFCs under dry reforming of methane are reported by Assabumrungrat and coworkers [27], and in other previous studies [51,53,59]. Feeding an equi-molar ratio of carbon dioxide and methane could be a risk for SOFC stability in long term operation, as shown in a durability test on a Ni-based anode supported SOFC operating at 800 °C and 0.3 A cm^{-2} [26].

In this context, since the general proportions of biogas from anaerobic digestion after cleaning of the impurities are typically 60% methane and 40% carbon dioxide on a volumetric basis [60] (i.e. a considerable amount of the CO_2 reforming agent is already available within the biogas) the direct feeding of SOFCs with biogas represents an interesting option for coupling a renewable source with a high efficiency conversion system [27,61]. Biogas from anaerobic digestion of organic residues, sewage sludge, municipal and industrial solid organic residues, liquid organic industrial effluents or farm residues is a relatively cheap, widely diffused and

often easily available fuel. One of the main drawbacks to the use of biogas in traditional power systems is its composition, which can vary dramatically according to location, season, biomass substrate and the biological process [57,62]. The composition of biogas usually lies within the following ranges (% vol.): 50–70% methane, 25–50% carbon dioxide, 1–5% hydrogen, 0.3–3% nitrogen hydrogen sulphide (H_2S) and various minor impurities [63]. Even though SOFCs have relatively high fuel flexibility, sulfur compounds can drastically reduce the catalytic/electro-catalytic properties of the anode electrode [35], siloxanes can deposit on catalyst surface, and halogens can reduce the Ni content in the electrode. Hence, the as-produced biogas needs impurities to be removed/reduced before feeding the SOFC. Therefore, desulfurization and the removal of other contaminants harmful to the SOFC (e.g., siloxanes and halogens) is an important step. Experimental studies show how the addition of air to the biogas reduces the risk of coking and enhances the stability of the biogas-fed SOFC [61,64]: another interesting option is the partial recirculation of the anode exhaust from the SOFC, making steam and carbon dioxide available for the conversion mechanism of methane.

The aim of this study is to explain in detail the dry reforming mechanism over Ni/YSZ anode, to determine the operating parameters (i.e., the carbon dioxide–methane molar ratio in the inlet mixture and the temperature) that achieve the best performance in terms of conversion into hydrogen and carbon monoxide, and to offer some practical conclusions for optimization of the process. In particular, a high carbon dioxide–methane ratio is recommended to ensure a carbon safe operating condition, even though it causes the dilution of the fuel, thus lowering the Nernst potential, the yield of hydrogen production and consequently the system efficiency [27,65]. Hence, the minimum carbon dioxide–methane molar ratio (for a fixed operating temperature and catalyst) required to operate the SOFC in a carbon-free condition is established from a detailed experimental investigation. The detailed study of this process can be useful for operation of a direct biogas SOFC. The further addition of carbon dioxide (coming from other processes or from recirculation of the exhaust gases of the SOFC, for instance combined with steam) to the as-received biogas feed could represent a possible option to operate SOFCs under direct internal reforming of biogas, whilst avoiding carbon formation.

2. Experimental

Compounds and elements (in molar content) coming out from the reactor are indicated by their chemical symbol (e.g., CH_4, CO_2), those in the inlet mixture are indicated by the addition of the suffix "$_{,i}$" (e.g., $CH_{4,i}$, $CO_{2,i}$), whereas species in the equilibrium composition calculated by software are indicated with the suffix "$_{,eq}$" (e.g., $CH_{4,eq}$, $CO_{2,eq}$).

The relative conversion of methane is defined as the ratio between the methane converted ($CH_{4,i}-CH_4$) and the methane in the inlet mixture ($CH_{4,i}$) and is indicated by the symbol "$CH_{4,rel.conv}$".

The study of the catalytic properties of the anode material is carried out with the same experimental apparatus described in detail by Lanzini et al. [26] and similar to test rigs previously used in other experiments [66,67]. Fragments of the anode (~5 mm*4 mm*0.53 mm) are placed in the catalyst bed of the micro-reactor apparatus. The anode material used is a NiO/8YSZ cermet. It is sintered for 2 h at 1500 °C, and is reduced before the experiments, by providing a mixture of 10% vol. hydrogen in Argon and increasing the reactor temperature from ambient temperature till 800 °C at a rate of 10 °C min^{-1}. Experiments are performed at ambient pressure with different amounts of anode to evaluate the influence of this factor (i.e., the influence of the gas residence time). Argon is the carrier gas used in all the experiments and the total flow rate (i.e., the amount of Ar plus the mixture of methane and carbon dioxide) of the inlet gas provided to the reactor is always kept constant at 100 ml min^{-1}. The kinetics and stability of the reactions over the employed anode are investigated by means of:

- Isotherm reactions (IsoT) at 800 °C conducted with two different procedures:
  - fixed mass of anode and carbon dioxide–methane molar ratio ($CO_{2,i}/CH_{4,i}$), the effect of the methane flow rate provided to the reactor ($CH_{4,i}$) is investigated;
  - fixed the mass of anode and $CH_{4,i}$, the effect of $CO_{2,i}/CH_{4,i}$ is investigated.
- Experiments studying the effect of the mass of the anode on the conversion;
- Temperature-programmed reactions (TPRx), increasing the temperature from ambient temperature to 800 °C. The effect of different rates of variation of the temperature with time (°C min^{-1}) is also investigated;
- Durability experiment with fixed flow rates and gas mixture composition at 800 °C.

The experimental results on the chemical composition obtained in IsoT and TPRx through the mass spectrometer (MS) are compared to the composition at chemical equilibrium conditions with the same inlet gas mixture and temperatures. The chemical equilibrium composition is calculated with the total Gibbs energy minimization method with the CEA software (Chemical Equilibrium with Applications [68]).

A list of the reactions, cited in the paper to describe the mechanism occurring during the experiments, is reported below:

	Reaction	ΔH^0 (kJ mol^{-1})
Dry reforming	$CH_4 + CO_2 = 2CO + 2H_2$	247 (1)
Water gas shift (WGS)	$CO + H_2O = CO_2 + H_2$	−40 (2)
Methane cracking	$CH_4 = C + 2H_2$	75 (3)
CO disproportionation (or Boudouard)	$2CO = C + CO_2$	−171 (4)
Steam/carbon gasification	$C + H_2O = CO + H_2$	131 (5)

3. Results

All the samples of NiO/YSZ are reduced in the catalytic bed before running the experiments with methane. Fig. 1 shows the volumetric flow rate coming out from the reactor during the reduction of ~280 mg of the anode sample (the trend in Fig. 1 shows well defined peaks because of the large amount of anode available; similar trends with smaller peaks are observed for lower amounts of anode in other experiments under the same conditions).

Two sharp peaks that are attributed to steam production (slightly shifted compared with the corresponding signal variation due to hydrogen consumption) are clearly visible at around 500 °C and after the end of the ramp at 800 °C, respectively. A similar trend is shown by Baker et al. [66] in a TPRd test (in 5% hydrogen in Helium) with NiO/YSZ. The first peak is characteristic of a NiO/YSZ cermet treated with a sintering process at high temperature. The peak at 800 °C is likely due to the large decrease in surface area through the agglomeration of particles on sintering.

A representation of the position of most of the examined mixtures in the carbon–hydrogen–oxygen ternary diagram is given in Fig. 2. Furthermore, boundaries of the carbon deposition region for different temperature are plotted.

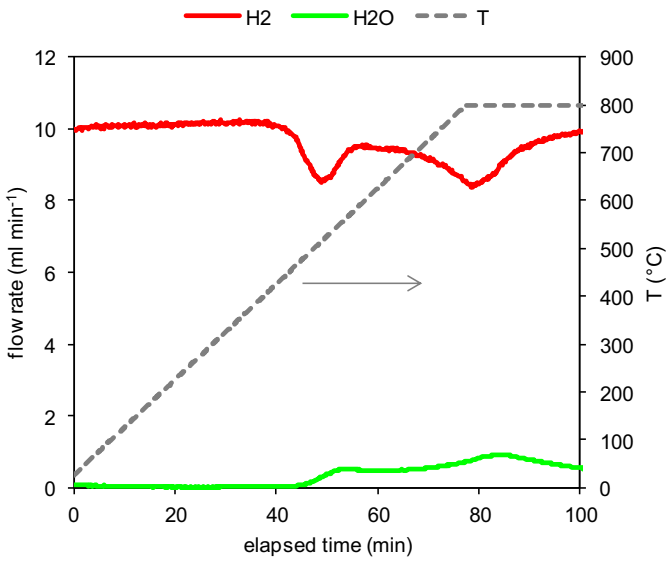

Fig. 1. Temperature Programmed Reduction (TPRd) of ~280 mg of NiO/YSZ.

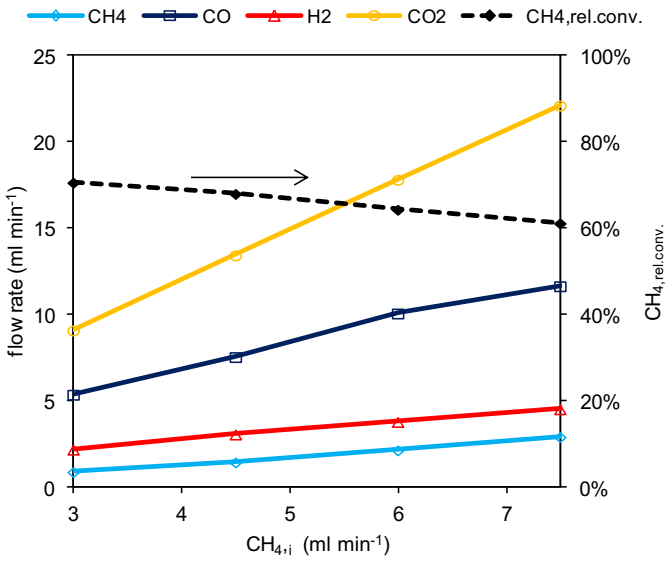

Fig. 3. Outlet gas mixture composition at 800 °C for $CO_{2,i}/CH_{4,i}$ = 4 (~70 mg of anode).

3.1. Isotherm reactions (IsoT) at 800 °C

The temperature fixed for the Isotherm reactions experiments is always 800 °C, which is a typical operating temperature for SOFCs.

3.1.1. IsoT fixed the $CO_{2,i}/CH_{4,i}$ ratio, varying $CH_{4,i}$

Fig. 3 shows the catalytic conversion for $CO_{2,i}/CH_{4,i}$ = 4 and different methane flow rates ($CH_{4,i}$). In the secondary *y*-axis, the relative conversion of methane ($CH_{4,rel.conv.}$) is shown. The water vapor concentration is not shown in any of the plots because its signal is unreliable for the multiple compound mixtures used in this experiment and detected with this experimental apparatus.

The quantity of each gas product at the outlet of the reactor is almost proportional to $CH_{4,i}$. $CH_{4,rel.conv.}$ is always higher than 60%, and it is decreasing for enhanced flow rates of methane because

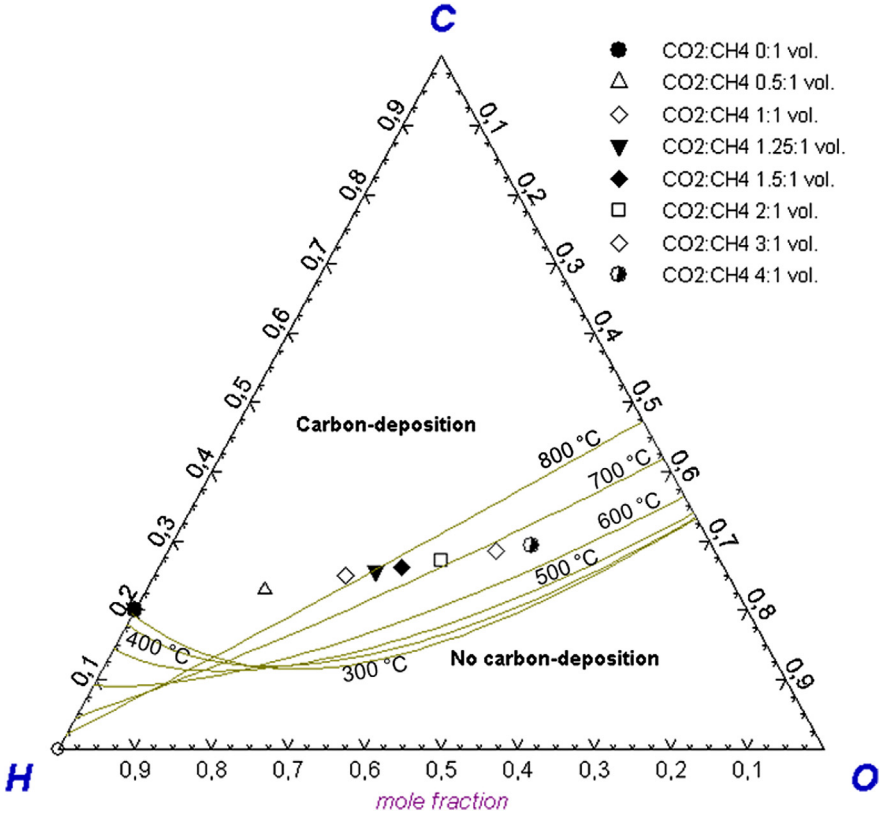

Fig. 2. Position of the mixtures of inlet gases in the carbon–hydrogen–oxygen chemical equilibrium diagram. Boundaries of the carbon deposition region for the different temperatures are obtained using Factsage software.

there is a higher fuel flow rate to convert for the same mass of catalyst and total flow rate. In Fig. 4, the response of this experiment for different $CO_{2,i}/CH_{4,i}$ ratios is compared.

The increase of the reaction products is linear with $CH_{4,i}$ (as in Fig. 3) for all ratios, except for the case with pure methane ($CO_{2,i} = 0$) where the amount of reaction product is negligible and almost all the methane remains unconverted. Conversion is poor for $CO_{2,i}/CH_{4,i} < 1$: pure methane provided to the reactor has a $CH_{4,rel.conv.}$ lower than 10% and, for $CO_{2,i}/CH_{4,i} = 0.5$, $CH_{4,rel.conv.}$ is not higher than 30% (result not shown in Fig. 4). $CH_{4,rel.conv.}$ is instead much higher and has the same order of magnitude for $CO_{2,i}/CH_{4,i} = 1$ and higher. It is evident that the conversion mechanism and the reactions involved are strongly dependent on $CO_{2,i}/CH_{4,i}$. The following plots give another representation and explanation of this behavior.

3.1.2. *IsoT fixed the $CH_{4,i}$, varying $CO_{2,i}/CH_{4,i}$*

In Fig. 5(a)–(c), with $CH_{4,i} = 6$ ml min^{-1}, the effect of varying the $CO_{2,i}/CH_{4,i}$ ratio is shown for experiments with different masses of catalyst (similar trends are obtained for all experiments conducted in a range of $3 < CH_{4,i} < 7.5$ ml min^{-1}, with slight differences in composition due to the different flow rates of gas). On the *y*-axis the concentration of the species is normalized, dividing the volumetric flow rates by the inlet methane flow rate ($CH_{4,i}$).

The plots in Fig. 5 suggest two different conversion mechanisms depending on the $CO_{2,i}/CH_{4,i}$ ratio:

- for $CO_{2,i}/CH_{4,i} < 1$, the catalytic activity of the anode is low: the relative conversion of methane is almost negligible in the case of a pure methane feed for both Fig. 5(a) and (b) (pure methane provided to the reactor is indicated in the plot by $CO_{2,i}/CH_{4,i} = 0$); $CH_{4,rel.conv.} \sim 20\%$ for $CO_{2,i}/CH_{4,i} = 0.5$ in the experiment of Fig. 5(a), whereas $CH_{4,rel.conv.} \sim 30\%$ for Fig. 5(b), as already discussed in Fig. 4. For $CO_{2,i}/CH_{4,i} = 0.5$, a small amount of H_2 and CO is formed. The molar contents of the two species are very close to each other; hence the main reaction involved in these conditions is probably the dry reforming reaction (1).

The high amount of anode of the experiment in Fig. 5(c) (gas residence time $= 2.8 \times 10^{-3}$ g min cm^{-3}) allows a much higher

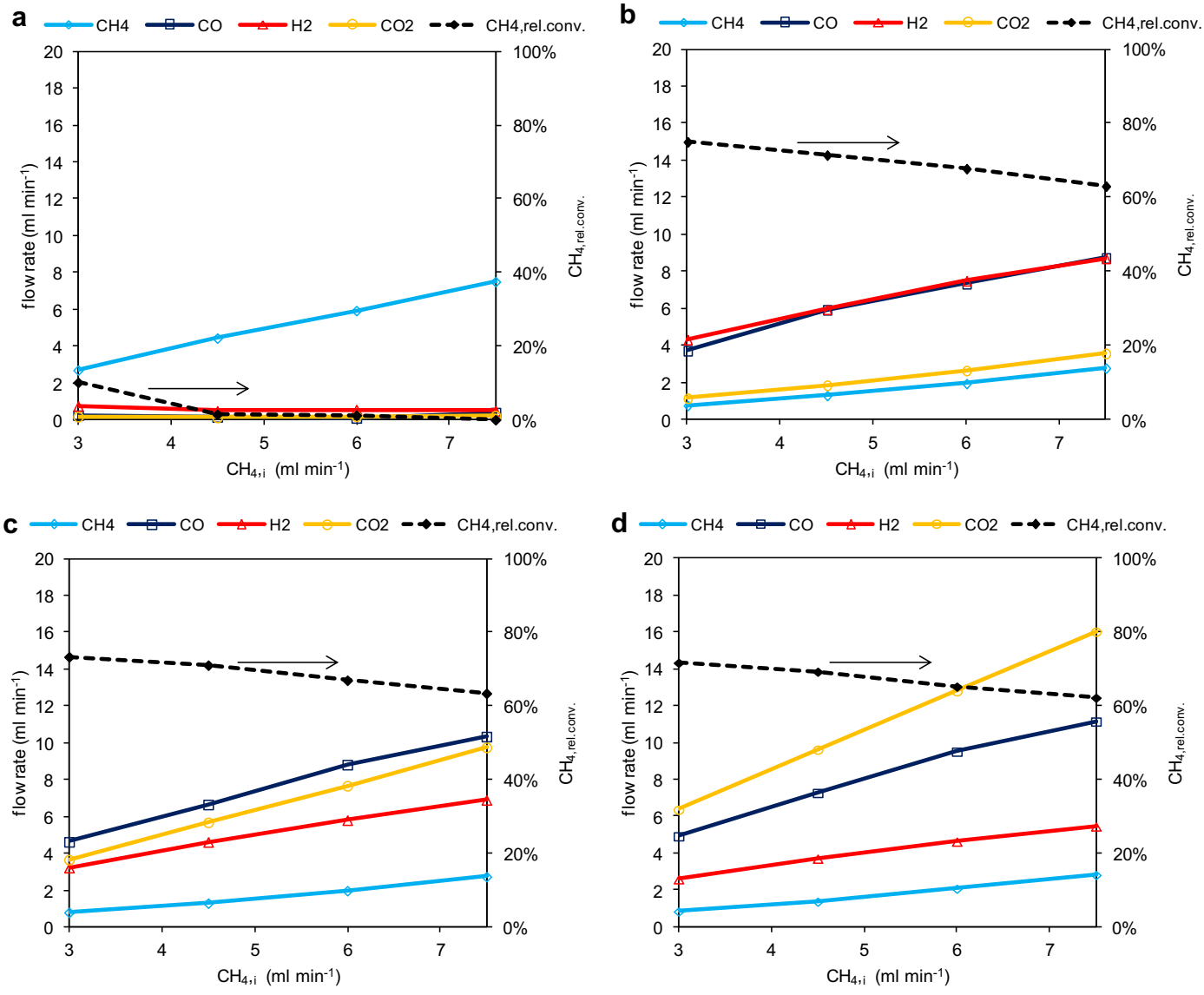

Fig. 4. Comparison of the outlet gas composition at 800 °C (~70 mg): (a) pure $CH_{4,i}$; (b) $CO_{2,i}/CH_{4,i} = 1$; (c) $CO_{2,i}/CH_{4,i} = 2$; (d) $CO_{2,i}/CH_{4,i} = 3$.

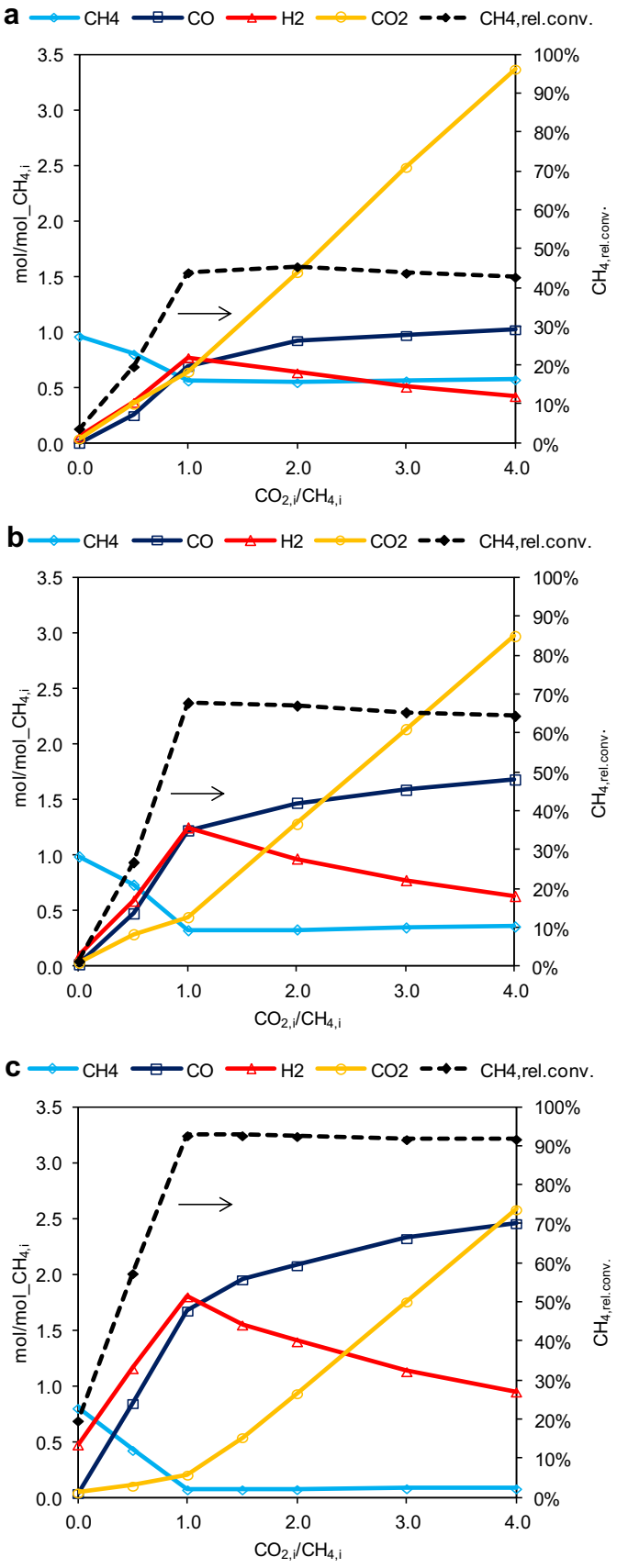

Fig. 5. Outlet gas mixture composition at 800 °C for $CH_{4,i}$ = 6 ml min^{-1} varying the $CO_{2,i}/CH_{4,i}$ ratio with: (a) ~35 mg; (b) ~70 mg; (c) ~280 mg.

conversion (as expected) comparing with the previous cases: for pure methane $CH_{4,rel.conv.}$ is not negligible (~20%), the amount of H_2 in the outlet mixture is about two times the amount of methane consumption ($CH_{4,i}$–CH_4). For $CO_{2,i}/CH_{4,i}$ = 0.5, the amount of H_2 is slightly higher than CO (whereas the difference between H_2 and CO was negligible in the previous cases). This data suggests that the partial activation of reaction (3), along with dry reforming reaction (1) (already pointed out in the previous cases with lower mass of anode), is the most probable explanation of this behavior.

- for $CO_{2,i}/CH_{4,I} \geq 1$, the catalytic activity is much higher than in the studies reported above, and almost constant with increasing ratio of $CO_{2,i}/CH_{4,i}$. The dominant reactions involved are dry reforming (1) and water gas shift (2). With increasing $CO_{2,i}/CH_{4,i}$, the content of $CO_{2,i}$ reacting (i.e., $CO_{2,i}$–CO_2) and CO produced, increases, whereas the content of H_2 decreases: this shows that the equilibrium of dry reforming (1) is kept in the forward direction (equilibrium constant very high), whereas the equilibrium of reaction (2) is moved backwards. This behavior is due to the equilibrium constant of the water gas shift reaction (2), which is close to 1 at 800 °C, hence a different amount of reactants can strongly affect the mixture composition, moving the reaction in one direction or the other. As expected, Fig. 5(c) shows the same trends as Fig. 5(a) and (b), with a different molar contents of the products, depending on the different methane conversion (for $CO_{2,i}/CH_{4,I} \geq 1$, $CH_{4,rel.conv.}$ ~45% in Fig. 5(a), $CH_{4,rel.conv.}$ ~65% in Fig. 5(b), $CH_{4,rel.conv.}$ ~92% in Fig. 5(c)).

Fig. 6 shows the calculated equilibrium composition for the same inlet mixture of gases at 800 °C.

This shows almost full relative conversion of methane ($CH_{4,rel.conv.}$ = 1) for all ranges of $CO_{2,i}/CH_{4,i}$ at equilibrium conditions. Two different regions are clear in Fig. 6:

- for $CO_{2,i}/CH_{4,i} < 1.25$, there is solid carbon formation (indicated in the plot by "C"), a high content of H_2, at all conditions, and a CO content which increases with $CO_{2,i}/CH_{4,i}$, probably due to methane cracking reaction (3) and the dry reforming reaction (1), with the latter gradually becoming dominant with increasing of $CO_{2,i}/CH_{4,i}$.

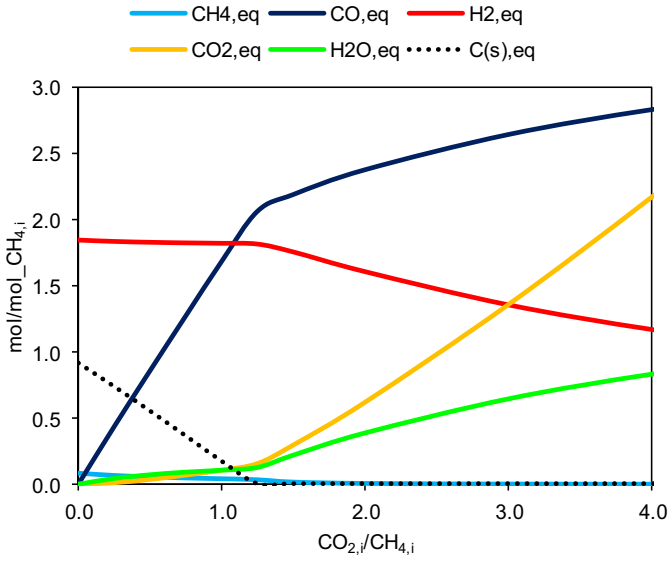

Fig. 6. Chemical equilibrium composition calculated for a mixture of methane and carbon dioxide at 800 °C varying $CO_{2,i}/CH_{4,i}$.

- for $CO_{2,i}/CH_{4,i} \geq 1.25$, the equilibrium composition shows the same trends as the experimental results, showing that the behavior of the water vapor signal fits the assumption of the equilibrium of water gas shift reaction (2) moved backwards with increasing ratio of $CO_{2,i}/CH_{4,i}$.

The equilibrium composition data of Fig. 6 are consistent with the results obtained in other studies [27,51,69].

The concentration of CH_4, CO, H_2 and CO_2 in Fig. 5(c) and Fig. 6 is shown in the same plot in Fig. 7.

From the comparison of the experimental and equilibrium results, it is possible to state that the conversion of methane for $CO_{2,i}/CH_{4,i} < 1$ is much lower than for the higher range because the cracking reaction is not well catalyzed. For $CO_{2,i}/CH_{4,i} > 1$, the experimental values of the flow rates of CH_4, CO, H_2 and CO_2 using ~280 mg of anode are close to the equilibrium values, with small differences mainly due to the partial conversion of methane (~92%) and other minor experimental errors.

Therefore, the investigated material is not a good catalyst for the cracking reaction, which has the positive implication of reducing the risk of deactivation of the catalyst in a carbon deposition region, whereas it is a good catalyst for the reactions of the dry reforming reaction (1) and the water gas shift reaction (2) at 800 °C for a $CO_{2,i}/CH_{4,i}$ ratio higher than a certain threshold (~1). According to the equilibrium composition at 800 °C, solid carbon formation is avoided for $CO_{2,i}/CH_{4,i} > 1.25$. As mentioned before, local temperature gradients and the non-homogeneous distribution of reactants and products can lead to carbon deposition, even when carbon is not thermodynamically predicted. Hence, a conservative condition to perform long term experiments in a carbon safe region should be $CO_{2,i}/CH_{4,i} > 1.5$. As stated before, for $CO_{2,i}/CH_{4,I} > 1$, the extra addition of carbon dioxide in the inlet mixture has no further beneficial effects on the global amount of fuel (H_2 and CO), reducing the amount of hydrogen and increasing the carbon monoxide in the outlet composition. Furthermore, an excess of carbon dioxide (and in general of the oxidant agent) might increase the risk of Ni re-oxidation in portions of the anode and can be detrimental on the cell long-term operation. Therefore, an optimal ratio for the catalytic conversion of a mixture of methane and carbon dioxide on the employed anode, based on Ni/YSZ, is in the range: $1.5 < CO_{2,i}/CH_{4,i} < 2$.

3.2. Temperature programmed reactions (TPRx)

The TPRx experiments in this work look at the effect of different temperature ramp rates on the composition of the outlet mixture, keeping all the other parameters constant: $CO_{2,i}/CH_{4,i} = 4$, $CH_{4,i} = 3$ ml min^{-1}, mass of anode ~280 mg. The ramps studied are in the range between 5 °C min^{-1} and 20 °C min^{-1} but only results obtained with these extremes are shown.

The behavior of Fig. 8(a) and (b) is almost equal, therefore the kinetics of the reactions are fast enough to be independent of the ramp rates, depending only on temperature. After the temperature reaches the set-point of 800 °C, the outlet mixture composition remains almost constant, and the concentration values of all species are equal to the corresponding values obtained from other experiments performed under the same conditions, shown in Fig. 6(b). Hence, the final composition of the mixture is independent of the sequence of the experiments (in Fig. 8(a), $CH_{4,i} = 3$ ml min^{-1}, whereas in Fig. 6(b) $CH_{4,i} = 6$ ml min^{-1} but all experiments with the typology described in 3.1.2 show similar results for different $CH_{4,i}$, as already stated). A comparison of the

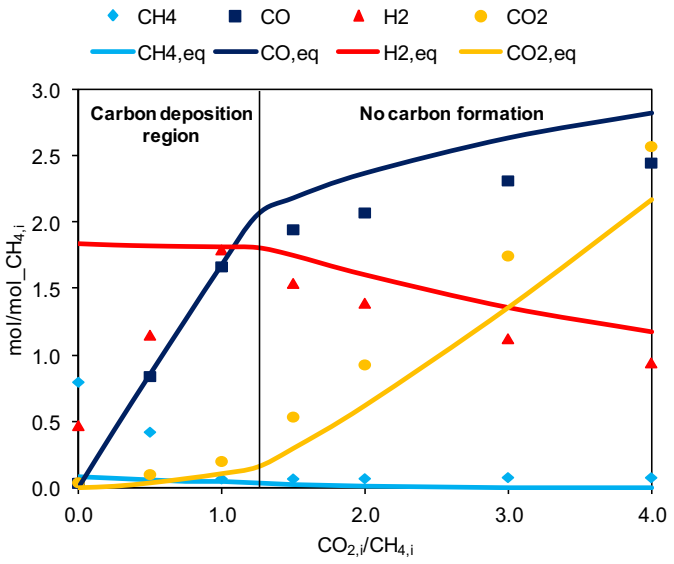

Fig. 7. CH_4, CO, H_2 and CO_2 flow rates for $CH_{4,i} = 6$ ml min^{-1} (~280 mg) and chemical equilibrium composition calculated at 800 °C with varying $CO_{2,i}/CH_{4,i}$ ratio.

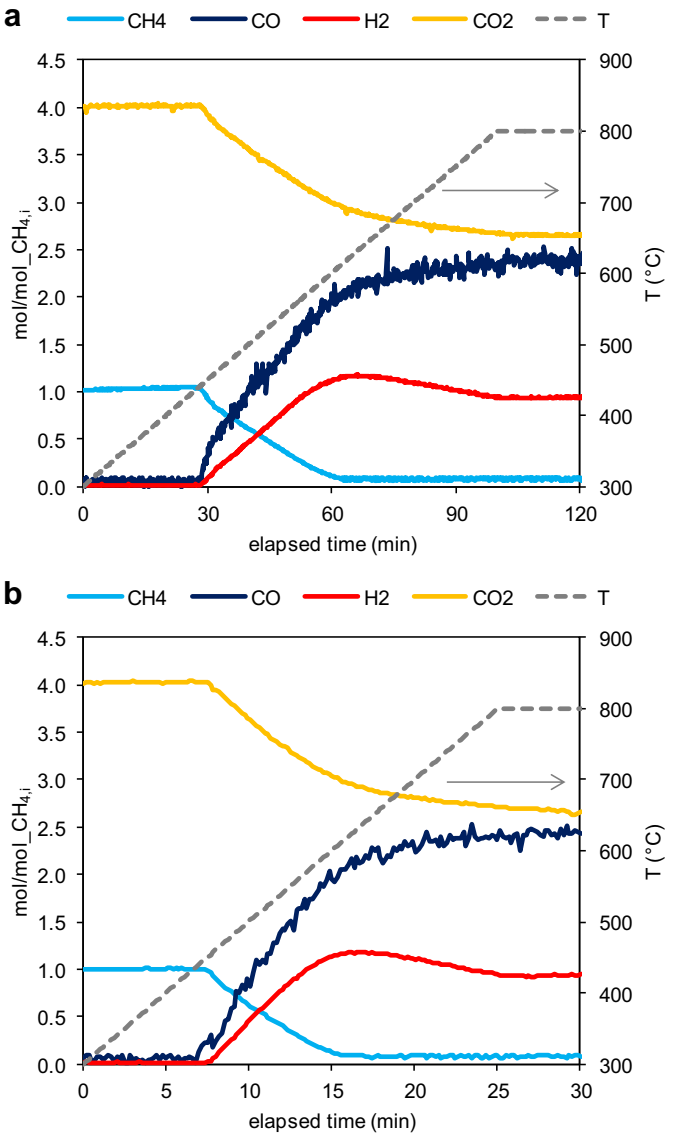

Fig. 8. Temperature programmed reactions for $CO_{2,i}/CH_{4,i} = 4$, $CH_{4,i} = 3$ ml min^{-1} (~280 mg): (a) ramp at 5 °C min^{-1}; (b) ramp at 20 °C min^{-1}.

experimental composition and that calculated at chemical equilibrium as a function of temperature is shown in Fig. 9.

Fig. 9(a) shows that the conversion of methane, for fixed $CH_{4,i}$ and $CO_{2,i}/CH_{4,i} = 4$, is negligible for $T < 450$ °C and increases for higher temperatures, reaching $CH_{4,rel.conv.} > 90\%$ at ~700 °C. Three distinct regions are clear:

- for $T < 450$ °C, the catalytic activity is poor;
- for 450 °C $< T <$ ~620 °C (where the H_2 peak is located), the concentration of CH_4 and CO_2 slightly decreases (CH_4 decreases with a slope smaller than that of CO_2), H_2 and CO slightly increase and the difference between CO and H_2 increases with the temperature. Dry reforming (1) and the reverse of the water gas shift reaction (2) determine this behavior;
- for $T >$ ~620 °C, there is a high and almost constant methane conversion ($CH_{4,rel.conv.} > 90\%$), CO_2 continues to slightly decrease (with a smaller slope compared to the previous region), H_2 slightly decreases and CO increases (again with a smaller slope compared to the previous region): the equilibrium of the water gas shift reaction (2) is further moved backward.

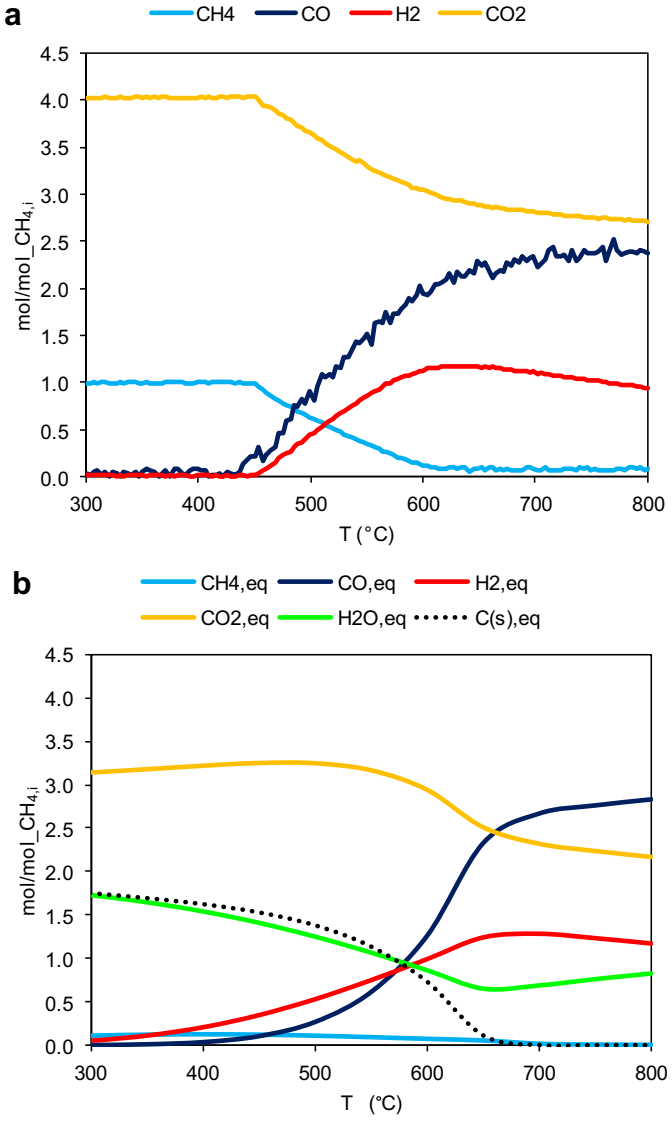

Fig. 9. TPRx for $CO_{2,i}/CH_{4,i} = 4$: (a) $CH_{4,i} = 3$ ml min^{-1} (~280 mg); (b) chemical equilibrium composition calculated for $CO_{2,i}/CH_{4,i} = 4$.

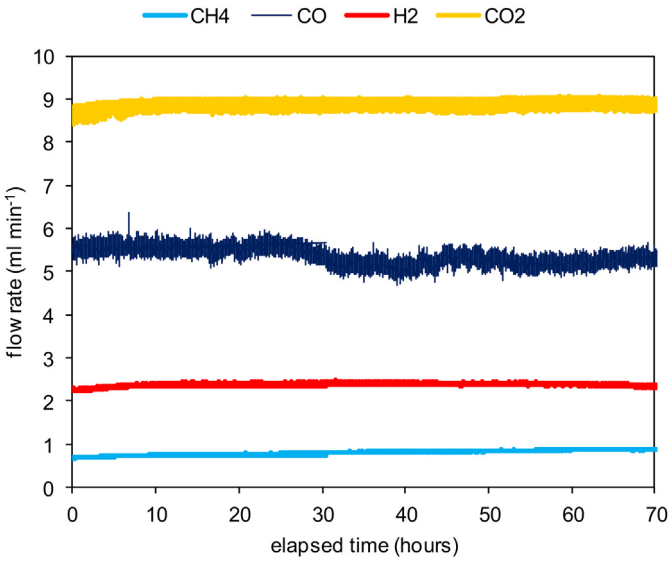

Fig. 10. Durability test for $CH_{4,i} = 3$ ml min^{-1}, $CO_{2,i}/CH_{4,i} = 4$, at 800 °C (~70 mg).

The main difference between the experimental results in Fig. 9(a) and the calculated equilibrium composition in Fig. 9(b) is observed for the first region ($T < 450$ °C), where high conversion of methane ($CH_{4,rel.conv.} > 85\%$) is expected, with the consumption of a certain amount $CO_{2,i}$ and the production of water vapor and solid carbon. Water vapor and solid carbon gradually decrease with increasing temperature, and are substituted by the same products described for Fig. 9(a). The amount of solid carbon in Fig. 9(b) would probably derive, at equilibrium conditions, from the combination of dry reforming (1) and the reverse of the steam/carbon gasification reaction (5). Reaction (5) is favored and is probably faster than the other carbon formation reactions ((3) and (4)) at low temperatures [70,71]. Combining all the previous information, the experimental results of Fig. 9(a) suggest that the dry reforming reaction (1) is not activated for temperatures lower than 450 °C.

The employed material can be considered a good catalyst for the dry reforming reaction (1) and water gas shift reaction (2) (due to almost full conversion of methane and produced H_2 and CO levels not far from the equilibrium composition) for temperatures higher than 620 °C. However, according to the calculated equilibrium composition, solid carbon formation is avoided for temperature higher than 650 °C.

3.3. Durability test

A short term durability test is performed, fixing the following parameters: $CH_{4,i} = 3$ ml min^{-1}, $CO_{2,i}/CH_{4,i} = 4$, ~70 mg at 800 °C. The result is shown in Fig. 10.

The catalytic conversion is stable over the testing period of 70 h: the investigated material shows no degradation or deactivation of the catalytic properties under these conditions, though clearly more extensive testing is required before technologically relevant conclusions can be drawn regarding lifetime.

4. Discussion

The Ni/YSZ anode samples have been studied in the micro-reactor apparatus under a mixture of methane and carbon dioxide. The ratios in the range $1.5 < CO_{2,i}/CH_{4,i} < 2$ allow to obtain the highest methane conversion and the highest concentration of fuel (hydrogen and carbon monoxide) in the mixture leaving the micro-

reactor, while keeping the operating condition in a carbon safe region. This result makes biogas an interesting candidate as fuel for running SOFCs: the addition of carbon dioxide (provided from other processes or, for instance, from a partial recirculation of the exhaust) to the significant amount already available in the inlet feed stream of purified biogas can allow the optimization of performances, ensuring long term stability. Nevertheless, this is an optimal range just in terms of the catalytic conversion under no current load and can be slightly different from the optimal ratio during the operation of the SOFC system. As already stated, the current load can help to prevent carbon deposition phenomena and can allow operations with lower ratios due to the backflow of the electrochemical reaction products and the direct oxidation of carbon deposited on the anode. For example, as mentioned before, some works show the best performances of the SOFC system for a ratio close to the equi-molar. The theoretical effect of the current load can be visible in the carbon–hydrogen–oxygen ternary diagram [25]. Under current load, the position of the mixture of inlet gases is moved toward the "O" (oxygen) vertex (due to the oxygen ions, which react at the anode side under current load), that is closer to the carbon safe region.

Furthermore, during the SOFC operation, the presence of the endothermic reforming reactions can cause local temperature gradients, especially at the fuel inlet side. Stress concentration can take place in minimum temperature points. In these cold spots, the oxidant/fuel ratio can be insufficient to avoid carbon build-up, local concentrations of solid carbon can be produced and, in the worst case, the thermal stress can cause cell fracture. The addition of a content of air to the carbon dioxide/methane mixture (or biogas) is an interesting option. This choice has been investigated in some recent works [64,72] and it is effective both to avoid carbon deposition and to reduce the temperature gradients (because of the reactions of partial and total oxidation of methane, which are exothermic), without large loss of electrical efficiency.

5. Conclusions

The catalytic properties of Ni/YSZ anode under dry reforming of methane have been investigated. Temperature Programmed Reactions show that the catalytic activity is poor for temperatures lower than 450 °C, because the dry reforming reaction is not catalyzed, whereas, for higher temperatures, the employed material is a good catalyst for both the dry reforming and reverse water gas shift reactions. For a gas residence time of 2.8×10^{-3} g min cm^{-3} and temperatures higher than 620 °C, the system goes close to equilibrium. Isotherm reactions at 800 °C show high catalytic activity for all the carbon dioxide–methane ratios equal or higher than equi-molar, whereas, for lower ratios, conversion is poor due to the low catalytic activity of this material toward the methane cracking reaction. At 800 °C, an optimal molar ratio for the catalytic conversion of a mixture of methane and carbon dioxide in hydrogen and carbon monoxide is 1.5 < carbon dioxide/methane < 2. Stable conversion performance is maintained over a test period of 70 h.

References

[1] S.C. Singhal, Solid State Ionics 135 (2000) 305–313.
[2] A. Atkinson, S. Barnett, R.J. Gorte, J.T. Irvine, A.J. McEvoy, M. Mogensen, S.C. Singhal, J. Vohs, Nat. Mater. 3 (2004) 17–27.
[3] C. Song, Catal. Today 77 (2002) 17–49.
[4] N.P. Brandon, S. Skinner, B.C.H. Steele, Ann. Rev. Mater. Res. 33 (2003) 183–213.
[5] X. Wang, Y. Ma, R. Raza, M. Muhammed, B. Zhu, Electrochem. Commun. 10 (2008) 1617–1620.
[6] R. Raza, X. Wang, Y. Ma, X. Liu, B. Zhu, Int. J. Hydrogen Energy 35 (2010) 2684–2688.
[7] T. Hibino, A. Hashimoto, T. Inoue, J.-i. Tokuno, S.-i. Yoshida, M. Sano, Science 288 (2000) 2031–2033.
[8] N.Q. Minh, T. Takahashi, Science and Technology of Ceramic Fuel Cells, Elsevier, Amsterdam, 1995.
[9] N.Q. Minh, J. Am. Ceram. Soc. 76 (1993) 563–588.
[10] B.C.H. Steele, A. Heinzel, Nature 414 (2001) 345–352.
[11] O. Yamamoto, Electrochim. Acta 45 (2000) 2423–2435.
[12] D.J.L. Brett, A. Atkinson, N.P. Brandon, S.J. Skinner, Chem. Soc. Rev. 37 (2008) 1568–1578.
[13] S.C. Singhal, K. Kendall, High Temperature and Solid Oxide Fuel Cells, Elsevier, Amsterdam, 2003.
[14] P. Aguiar, D. Chadwick, L. Kershenbaum, Chem. Eng. Sci. 57 (2002) 1665–1677.
[15] N. Laosiripojana, S. Assabumrungrat, Appl. Catal. B 60 (2005) 107–116.
[16] S. Park, R. Craciun, J.M. Vohs, R.J. Gorte, J. Electrochem. Soc. 146 (1999) 3603–3605.
[17] S. McIntosh, R.J. Gorte, Chem. Rev. 104 (2004) 4845–4865.
[18] R.J. Gorte, H. Kim, J.M. Vohs, J. Power Sources 106 (2002) 10–15.
[19] M.C. Tucker, G.Y. Lau, C.P. Jacobson, S.J. Visco, L.C. De Jonghe, J. Power Sources 195 (2010) 3119–3123.
[20] Y.-H. Huang, R.I. Dass, Z.-L. Xing, J.B. Goodenough, Science 312 (2006) 254–257.
[21] S. Tao, J.T.S. Irvine, Nat. Mater. 2 (2003) 320–323.
[22] M.C. Tucker, J. Power Sources 195 (2010) 4570–4582.
[23] A.L. Dicks, J. Power Sources 71 (1998) 111–122.
[24] V. Alzate-Restrepo, J.M. Hill, J. Power Sources 195 (2010) 1344–1351.
[25] J.-H. Koh, Y.-S. Yoo, J.-W. Park, H.C. Lim, Solid State Ionics 149 (2002) 157–166.
[26] A. Lanzini, P. Leone, C. Guerra, F. Smeacetto, N.P. Brandon, M. Santarelli, Chem. Eng. J. 220 (2013) 254–263.
[27] S. Assabumrungrat, N. Laosiripojana, P. Piroonlerkgul, J. Power Sources 159 (2006) 1274–1282.
[28] A. Lanzini, P. Leone, Int. J. Hydrogen Energy 35 (2010) 2463–2476.
[29] J.R. Rostrup-Nielsen, J. Sehested, J.K. Nørskov, Hydrogen and Synthesis Gas by Steam- and CO_2 Reforming, in: B.C. Gates, H. Knözinger (Eds.), Advances in Catalysis, Academic Press, Lyngby, 2002, pp. 65–139.
[30] C.H. Bartholomew, Catal. Rev. 24 (1982) 67–112.
[31] T. Takeguchi, Y. Kani, T. Yano, R. Kikuchi, K. Eguchi, K. Tsujimoto, Y. Uchida, A. Ueno, K. Omoshiki, M. Aizawa, J. Power Sources 112 (2002) 588–595.
[32] V. Sadykov, N. Mezentseva, G. Alikina, R. Bunina, V. Pelipenko, A. Lukashevich, S. Tikhov, V. Usoltsev, Z. Vostrikov, O. Bobrenok, A. Smirnova, J. Ross, O. Smorygo, B. Rietveld, Catal. Today 146 (2009) 132–140.
[33] E.P. Murray, T. Tsai, S.A. Barnett, Nature 400 (1999) 649–651.
[34] H. Sumi, Y.-H. Lee, H. Muroyama, T. Matsui, K. Eguchi, J. Electrochem. Soc. 157 (2010) B1118–P1125.
[35] Y. Shiratori, T. Oshima, K. Sasaki, Int. J. Hydrogen Energy 33 (2008) 6316–6321.
[36] N. Laosiripojana, W. Sutthisripok, S. Assabumrungrat, Chem. Eng. J. 112 (2005) 13–22.
[37] N. Laosiripojana, D. Chadwick, S. Assabumrungrat, Chem. Eng. J. 138 (2008) 264–273.
[38] D.H. Prasad, H.I. Ji, H.R. Kim, J.W. Son, B.K. Kim, H.W. Lee, J.H. Lee, Appl. Catal. B 101 (2011) 531–539.
[39] A.L. Sauvet, J.T.S. Irvine, Solid State Ionics 167 (2004) 1–8.
[40] T. Takeguchi, R. Kikuchi, T. Yano, K. Eguchi, K. Murata, Catal. Today 84 (2003) 217–222.
[41] A. Weber, B. Sauer, A.C. Müller, D. Herbstritt, E. Ivers-Tiffée, Solid State Ionics 152–153 (2002) 543–550.
[42] Y. Lin, Z. Zhan, J. Liu, S.A. Barnett, Solid State Ionics 176 (2005) 1827–1835.
[43] Y. Lin, Z. Zhan, S.A. Barnett, J. Power Sources 158 (2006) 1313–1316.
[44] S. Park, J.M. Vohs, R.J. Gorte, Nature 404 (2000) 265–267.
[45] J. Liu, S.A. Barnett, Solid State Ionics 158 (2003) 11–16.
[46] K.C. Wincewicz, J.S. Cooper, J. Power Sources 140 (2005) 280–296.
[47] N. Laosiripojana, S. Assabumrungrat, J. Power Sources 163 (2007) 943–951.
[48] D. Mogensen, J.D. Grunwaldt, P.V. Hendriksen, K. Dam-Johansen, J.U. Nielsen, J. Power Sources 196 (2011) 25–38.
[49] A.K. Avetisov, J.R. Rostrup-Nielsen, V.L. Kuchaev, J.H. Bak Hansen, A.G. Zyskin, E.N. Shapatina, J. Mol. Catal. A: Chem. 315 (2010) 155–162.
[50] W. Sangtongkitcharoen, S. Assabumrungrat, V. Pavarajarn, N. Laosiripojana, P. Praserthdam, J. Power Sources 142 (2005) 75–80.
[51] J.H. Edwards, A.M. Maitra, Fuel Process. Technol. 42 (1995) 269–289.
[52] S.-G. Wang, Y.-W. Li, J.-X. Lu, M.-Y. He, H. Jiao, J. Mol. Struct. Theochem 673 (2004) 181–189.
[53] J.R. Rostrup-Nielsen, J.H.B. Hansen, J. Catal. 144 (1993) 38–49.
[54] A. Erdohelyi, J. Cserenyi, F. Solymosi, J. Catal. 141 (1993) 287–299.
[55] G. Goula, V. Kiousis, L. Nalbandian, I.V. Yentekakis, Solid State Ionics 177 (2006) 2119–2123.
[56] Y. Shiratori, K. Sasaki, J. Power Sources 180 (2008) 738–741.
[57] J. Staniforth, R.M. Ormerod, Catal. Lett. 81 (2002) 19–23.
[58] K. Girona, J. Laurencin, J. Fouletier, F. Lefebvre-Joud, J. Power Sources 210 (2012) 381–391.
[59] J.N. Armor, Appl. Catal. A: Gen. 176 (1999) 159–176.
[60] S. Bari, Renew. Energy 9 (1996) 1007–1010.
[61] J. Van herle, Y. Membrez, O. Bucheli, J. Power Sources 127 (2004) 300–312.
[62] J. Staniforth, K. Kendall, J. Power Sources 71 (1998) 275–277.
[63] H.H. Jawurek, N.W. Lane, C.J. Rallis, Biomass 13 (1987) 87–103.
[64] Y. Shiratori, T. Ijichi, T. Oshima, K. Sasaki, Int. J. Hydrogen Energy 35 (2010) 7905–7912.

[65] A. Lanzini, P. Leone, M. Pieroni, M. Santarelli, D. Beretta, S. Ginocchio, Fuel Cells 11 (2011) 697–710.
[66] R.T. Baker, I.S. Metcalfe, Ind. Eng. Chem. Res. 34 (1995) 1558–1565.
[67] I.S. Metcalfe, R.T. Baker, Appl. Catal. A: Gen. 126 (1995) 297–317.
[68] S. Gordon, B.J. McBride, Computer Program for Calculation of Complex Chemical Equilibrium Compositions and Applications. NASA Reference Publication 1311 (1996). Cleveland.
[69] J. Gao, Z. Hou, H. Lou, X. Zheng, Dry (CO_2) Reforming, in: D. Shekhawat, J.J. Spivey, David A. Berry (Eds.), Fuel Cells, Elsevier, Amsterdam, 2011, pp. 191–221 [chapter 7].
[70] H.J. Grabke, R. Krajak, J.C. Nava Paz, Corros. Sci. 35 (1993) 1141–1150.
[71] H.J. Grabke, Mater. Corros. 49 (1998) 303–308.
[72] Y. Takahashi, Y. Shiratori, S. Furuta, K. Sasaki, Solid State Ionics 225 (2012) 113–117.